SCIENTIFIC REPORTS

OPEN

Ab initio inspired design of ternary boride thin films

Vincent Moraes[1], Helmut Riedl[1,2], Christoph Fuger[1], Peter Polcik[3], Hamid Bolvardi[4], David Holec[1] & P. H. Mayrhofer[1,2]

Received: 13 February 2018
Accepted: 1 June 2018
Published online: 18 June 2018

The demand to discover new materials is scientifically as well as industrially a continuously present topic, covering all different fields of application. The recent scientific work on thin film materials has shown, that especially for nitride-based protective coatings, computationally-driven understanding and modelling serves as a reliable trend-giver and can be used for target-oriented experiments. In this study, semi-automated density functional theory (DFT) calculations were used, to sweep across transition metal diborides in order to characterize their structure, phase stability and mechanical properties. We show that early transition metal diborides (TiB_2, VB_2, etc.) tend to be chemically more stable in the AlB_2 structure type, whereas late transition metal diborides (WB_2, ReB_2, etc.) are preferably stabilized in the W_2B_{5-x} structure type. Closely related, we could prove that point defects such as vacancies significantly influence the phase stability and even can reverse the preference for the AlB_2 or W_2B_{5-x} structure. Furthermore, investigations on the brittle-ductile behavior of the various diborides reveal, that the metastable structures are more ductile than their stable counterparts (WB_2, TcB_2, etc.). To design thin film materials, e.g. ternary or layered systems, this study is important for application oriented coating development to focus experimental studies on the most perspective systems.

Designing new materials is a highly relevant topic covering many different aspects, like discovering materials with entirely new properties (e.g., carbon-nanotubes), improving existing materials in use, (e.g., reduce costs or weight), or increasing biocompatibility or environmental sustainability. These examples are just a small fraction of the never-ending quest fueled by modern industry. The increasing computational power opens new fruitful approaches for materials design[1]. Trial and error can be supported (thus focused) or even replaced by fundamental and sophisticated knowledge-based methods using semi-automated density functional theory calculations to scan across entire material classes[2]. Nitride-based materials, as prototypes of protective thin films for cutting and milling tool applications, have been intensively studied from their binary systems (e.g., TiN, AlN, CrN)[3–5] up to their ternary[6,7] or even multinary systems[8,9]. For example, TiN and Ti-Al-N are two highly prominent representatives present widely used in industry (e.g., tooling, microelectronics, decorative purpose). Additionally, considerable research activities concentrate on further application-oriented improvement of these materials using different architectural designs, which will combine their beneficial properties or create entirely new features[10].

A rather new and extremely promising class of materials–with the potential to be used for many different applications ranging from superconductivity to wear- and corrosion-resistance–are borides[11,12]. Contrary to nitrides, only little is known about borides and more specifically about diborides, with the chemical formula XB_2 (where X stands for transition metals (TM)). While there are several experimental and theoretical studies on binary diborides[13,14], multinary diborides are rather unexplored[15–17]. Importantly, ReB_2 has been theoretically predicted to be the most incompressible material exceeding the properties of diamond suggesting the use in (iron alloys) cutting applications were traditional materials (e.g., diamond) cannot be used due to the formation of carbides[18,19]. A huge drawback, when considering TM-diborides for hard coating applications is the pronounced brittle behaviour of this material class. Hence, it is of great importance to classify their ductility and increase the toughness.

Many diborides tend to crystallize in two different hexagonal structures. While early transition metal diborides crystallize in the so-called AlB_2 structure type (α, space group 191 - P6/mmm)[2], late transition metal diborides (e.g., Tungstendiboride) prefer a W_2B_{5-x} based structure (ω, space group 194 - $P6_3/mmc$)[20] - see Fig. 1. The AlB_2 α-structure consists of a hexagonal shaped unit cell with an alternating stacking of covalently bonded

[1]Christian Doppler Laboratory for Application Oriented Coating Development at the Institute of Materials Science and Technology, TU Wien, A-1060, Wien, Austria. [2]Institute of Materials Science and Technology, TU Wien, A-1060, Wien, Austria. [3]Plansee Composite Materials GmbH, D-86983, Lechbruck am See, Germany. [4]Oerlikon Balzers, Oerlikon Balzers Surface Solutions AG, FL-9496, Balzers, Liechtenstein. Correspondence and requests for materials should be addressed to V.M. (email: vincent.moraes@tuwien.ac.at)

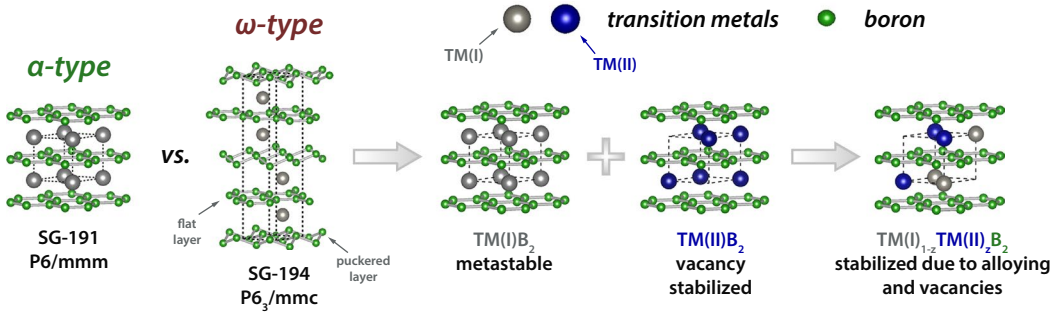

Figure 1. Competing structure types of transition metal diborides (α, space group 191, P6/mmm, vs. ω, space group 194, P6$_3$/mmc)[2,20] and possible phase stabilizing routes for AlB_2 structured diborides by alloying of a second transition metal and/or point defects (ternary boride).

graphite-like boron hexagons and metal layers. The closely related W_2B_{5-x} ω-structure type consists of hexagonal unit cell with alternating flat and puckered boron hexagons between the metal layers. Regarding the synthesis via physical vapor deposition, it is a well known fact, that metastable structures can be captured via this synthesis route[21,22], which is often achieved by the implementation of point defects such as vacancies[23,24]. This circumstance of depositing a metastable structure can lead to extraordinary and positive effects (e.g., AlN, which shows significantly higher mechanical strength and elastic constants for its metastable face centered cubic structure than its thermodynamically stable hexagonal close packed wurtzite-type structure) but includes also the fact that upon providing the necessary activation energy, the metastable structure will transform in its thermodynamically stable modification (which is well known and investigated for many of the metastable Al_2O_3 polymorphs that transform to corundum-type Al_2O_3). Here, materials science allows for at least two helpful scenarios: 1) decreasing the difference in Gibbs free energy between metastable and stable state (which decreases the driving force for the phase transformation) and 2) increasing the Gibbs free energy of the peak separating the metastable and stable state (which increases the necessary activation energy to reach the stable state.) Picking up the concept of ZrO_2 based ceramics, where alloying of certain elements (e.g., Mg, Y, Ce)[25] leads to stabilization of high temperature modifications at room temperature, the two hexagonal diboride phases draw a great starting point for the exploration of ternary diboride materials. The combination of these phase stabilizing routes for the preferred α-type structure are schematically depicted in Fig. 1. To use such concepts for designing new materials (not necessarily limited only to thin films), it is essential to know and understand the fundamental properties (e.g., energy of formation (E_f), lattice constants, etc.) of the building blocks. Furthermore, such a knowledge database allows to set-up target-oriented experiments aiming on fulfilling various demands.

In this study, we use density functional theory (DFT) to obtain basic properties of transition metal diborides (TMB_2) in their AlB_2 and W_2B_{5-x} structures (α-TMB_2 and ω-TMB_2). In addition to perfect structures we also investigate the impact of vacancies on the energy of formation (which characterizes the chemical stability) as materials prepared by physical vapor deposition techniques are known for their high density of point defects such as vacancies. Since mechanical properties are of central importance for protective coatings, we calculated the elastic constants (bulk and shear modulus, poisson ratio, and the cauchy pressure) of all these transition metal diborides (3 to 5d elements excluding Hg) in their α and ω crystal structure.

Results and Discussion

Ground state properties. The energy of formation E_f, which is a fundamental indicator (for chemical stability) of a solid matter, quantifies the energy gain (for negative E_f values) upon forming a compound out of the individual elements, calculated as:

$$E_f = \frac{1}{\sum_i n_i}\left(E_{tot} - \sum_i n_i E_i\right) \quad (1)$$

where, E_{tot} is the total energy of the compound (here, TMB_2), E_i the energy of the individual elemental constituent i in its stable crystalline configuration, and n_i denotes the number of atoms for the different species i. Figure 2 shows the energy of formation for all 28 TMB_2 materials calculated, spanning the whole range of 3d, 4d and 5d (excluding Hg) transition metals, in the two different but relevant hexagonal structures, α- and ω-type.

With increasing atomic number (within each period), the E_f values become less negative and even positive (i.e., chemically instable) for TMB_2 with Ni, Cu, Zn (3d elements), Pd, Ag, Cd (4d elements), Os, Ir, Pt, Au (5d elements). RuB_2 and RhB_2 (4d elements) are special border candidates as E_f is negative for their ω-structure but positive for their α-structure. The increasing chemical stability (i.e., more negative E_f values) with decreasing atomic mass (within the individual periods) underlines the increased reactivity of atoms with fewer valence electrons. Scandium and Yttrium slightly deviate from this tendency, which is comparable to the results obtained for nitrides[26].

The data also show that the early TMB_2 prefer the α-structure, which is in good agreement with earlier reports[16], and the largest difference in E_f between the α and ω structure of chemical stable TMB_2 is obtained for TiB_2, ZrB_2, and HfB_2, respectively. These results agree with the density of states (DOS), which show a pseudogap between the bonding and antibonding (TM-d and B-p) states. Within each period, the occupied bonding states change, to partially filled anti-bonding states with increasing atomic number. The decreasing $N(E_F)$ (number of

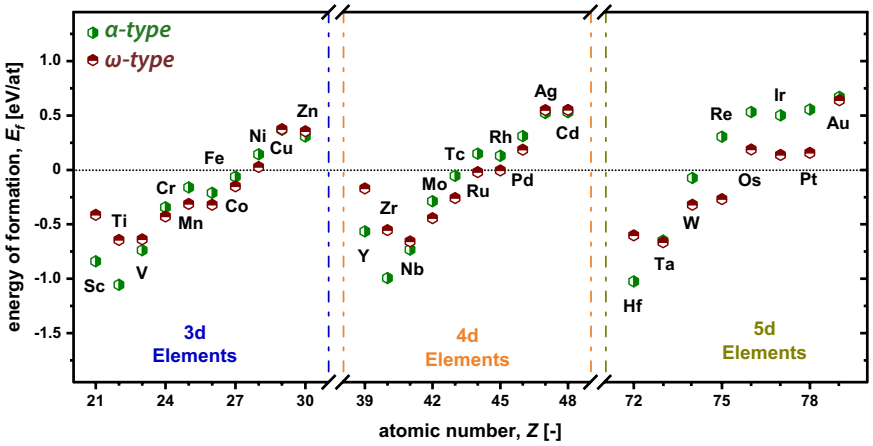

Figure 2. Energies of formation (E_f) per atom for all TMB_2 investigated (3d, 4d, and 5d transition metal elements, excluding Hg). The green and red hexagons represent the α- (AlB_2 prototype) and ω- (W_2B_{5-x} Prototype) type structures, respectively. Please not, that some diborides have very similar E_f in the two structure types and therefore overlapping symbols (e.g. Cu or Ta).

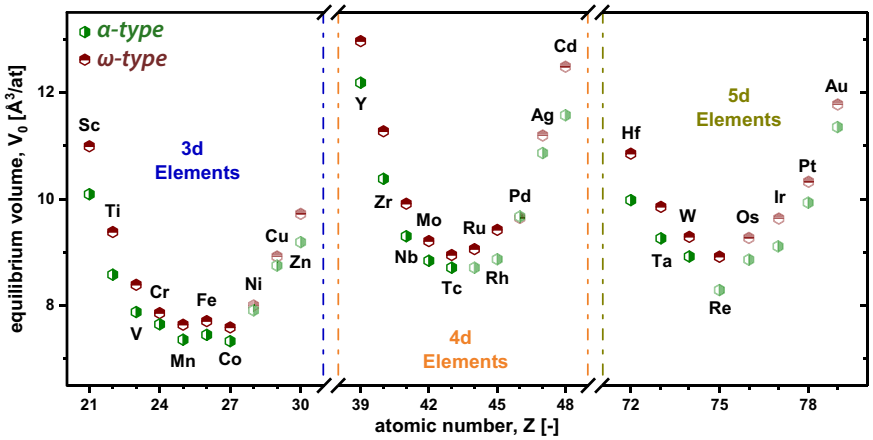

Figure 3. Equilibrium volumes for all TMB_2 obtained from fitting the Birch-Murnaghan equation. Green and red hexagons denote to euqilibrium volumes for α- and ω type, respectively. The elements showing positive E_f (see Fig. 2) are faded - starting at Ni, Ru, and Os for 3d, 4d, and 5d elements, respectively.

states at the fermi level (E_F) - corresponding to the position of the fermi level) reflects the chemical stability[27] and is in excellent agreement with literature reports[28–30]. Hence, in the case of α-structured TiB_2, ZrB_2, and HfB_2 the fermi level can be found in the pseudogap (lowest $N(E_F)$ - showing highest chemical stability), whereas for ScB_2 and YB_2 as well as VB_2, NbB_2, and TaB_2 the fermi level can be found in the bonding or antibonding states, respectively (reduced chemical stability). Furthermore, this circumstance also reflects the trend in melting temperatures (and the directionality of the bonding - covalent bonding character) for the individual diborides[31,32].

As expected from the presence of puckered B-planes in the W_2B_{5-x} structures, all ω-TMB_2 exhibit a higher equilibrium volume (and therefore lower mass density, which is not shown here) as compared to their corresponding α-TMB_2 relatives, see Fig. 3. The equilibrium volume decreases with the atomic radii (in each period), but only up to that transition metal where E_f becomes positive, please compare Figs 2 and 3. For higher atomic radii of the TM, the euquilibrium volume of the TMB_2 increases again.

In respect to the lattice parameters (shown in Fig. 4a,b) *a* and *c*, and their ratio (*c*/*a*), the trends are consistent for both structure types. For elements from the 3d period, lattice parameter *a* stays fairly constant whereas lattice parameter *c* draws a clear decrease. Therefore, the trend for the c/a-ratio is dominated by the change in *c* with increasing atomic number. Elements from the fourth period show a decrease in lattice constants *a* and *c* until MoB_2 for the α-structure and TcB_2 for the ω-structure. Hence, the c/a-ratio for the α-structure decreases to the point where the compounds energetically prefer the ω-structure. For the 5d elements both, the *a* and *c* lattice parameter, slightly decrease with increasing atomic number. α-VB_2 as well as α-CrB_2 even reveal a cubic-like c/a-ratio of ~1. Farenholtz *et al.*[33] stated, that the highly covalent B-B bonds are strong compared to TM-B or TM-TM bonds, which explains the small changes in lattice parameter a, with increasing atomic number (especially for the α-type). On the contrary, lattice parameter c is more dominated by the different atomic radii of the specific TM. Furthermore, stable α-TMB_2 are only formed with respect to strained B-B bonds (increased/

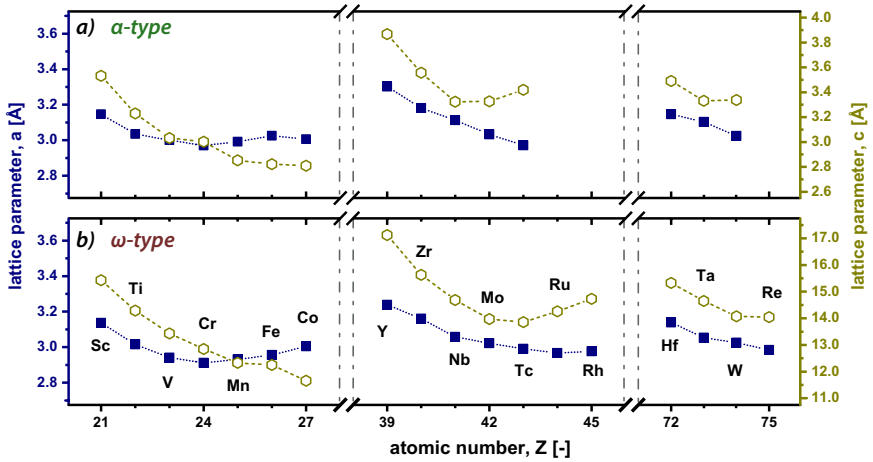

Figure 4. Lattice parameters *a* and *c* for all diborides studied, obtained from fitting the Birch-Murnaghan equation for stable structures (negative E_f). In (**a**) the lattice parameter for the α- and in (**b**) those for the ω-type structure are given.

decreased bonding length caused by the present TMs), which would be crucial for smaller TM-atoms as Cr or larger than Zr. The trends for the ω-type is a rather controversial discussed topic in literature and difficult to relate to experimental data. Several experimental and computational studies have been conducted treating the off-stoichiometry of this crystal structure (W_2B_{5-x}-prototype)[34,35]. Nevertheless, assuming perfect structures, the observed trends follow similar behavior as obtained for the α-type, which leads to the conclusion, that the presence of the puckered boron planes compensate the strain introduced by other TM-atoms such as Mo or W.

Mechanical properties. Outstanding mechanical properties, e.g. super- or ultra-hardness, strongly correlate to bonding types and hence strength. Fitting the total energy data obtained for variable volumes, with the Birch-Murnaghan equation of state, gives the bulk moduli quantifying the materials' resistance to isotropic pressure, and therefore represents a good guide for mechanical properties. The data (see Appendix S.1 and S.2) exhibit a maximum for each period as a function of the atomic number, which is at α-CrB_2 (B = 287 GPa), α-MoB_2 (B = 307 GPa), and ω-ReB_2 (B = 333 GPa), for the 3d, 4d, and 5d elements, respectively. Also within our study, ReB_2 exhibits the highest bulk modulus among all TMB_2 studied. This is in excellent agreement with literature, stating that ReB_2 is one of the hardest material available, approaching or even exceeding the excellent properties of diamond[18,19]. Comparing the maxima with the equilibrium volumes, their lowest volumes are at slightly higher atomic numbers, but within the chemically stable regions. As these ceramic-like TMB_2 materials exhibit a mixture of metallic, covalent, and ionic bonds, the bulk moduli maxima (which are within the chemically stable region, as mentioned) are an indication of stronger bonds leading also to smaller interatomic distances (represented by the specific volume). Generally, the α-TMB_2 exhibit higher bulk moduli than their ω-TMB_2 counterparts, corresponding to their smaller specific volumes, only MnB_2, TcB_2, and WB_2, slightly deviate, and FeB_2 strongly deviates from this trend.

The entire elastic tensor was calculated for all TMB_2 compounds in both structures, α and ω. These allow evaluating semi-empirical criteria for the ductile behavior. In this study, we use three different criteria: the Cauchy pressure (being C_{12}–C_{44}), the Pugh criteria (G/B ratio) as well as Frantsevich criteria on the Poisson ratio. After Pettifor *et al.*[36], a positive Cauchy pressure indicates a metallic bonding character, hence a ductile behavior. Consequently, a negative Cauchy pressure indicates a brittle behavior due to the directional bonding character (hence more covalent contribution). Frantsevich[37,38] and Pugh[39] introduced additional criteria to classify a brittle or ductile behavior, by using the Poisson ratio (ν) and the G/B ratio, respectively. A ductile behavior is obtained for $\nu > 0.26$ (Frantsevich criterion) or for $G/B < 0.57$ (Pugh criterion).

After these three criteria, presented in Fig. 5a (Frantsevich vs. Pugh criterion) and Fig. 5b (Pettifor vs. Pugh criterion), the most ductile ω-TMB_2 compounds are ZnB_2, PdB_2, NiB_2, and AuB_2, but these are actually chemically not stable (positive E_f and therefore not plotted in Fig. 5). All other ω-TMB_2 compounds are at the minimum of at least one criterion or are classified as brittle. Please note that within Fig. 5a,b not all data points are shown, namely ω type ScB_2, YB_2, RuB_2, as well as RhB_2, suggesting either extreme brittle or non-stable structures (more positive E_f as compared to their α type counterpart). The classical stable α-TMB_2, which exhibit a more negative E_f value than their ω-TMB_2 relatives - ScB_2, YB_2, TiB_2, ZrB_2, HfB_2, NbB_2 - are classified as brittle after all three criteria. Contrary to that, there are many chemically stable α-TMB_2 compounds, like MnB_2, FeB_2, CoB_2 (3d), and TcB_2 (4d), and WB_2 (5d), which are classified as ductile after all three criteria. Also α-MoB_2 as well as α-TaB_2 can be added to this list as it is ductile after Frantsevich and Pugh and only slightly brittle after Pettifor. These transition metal diborides actually prefer the ω-structure, but are believed to be stabilized in their α-structure by introducing point defects such as vacancies (see following sections). Here, the energetically barrier is very small for α-TaB_2, see Fig. 2.

Recalling Fig. 2, we see that the chemical stability (increases with decreased $N(E_F)$) is reflected in the brittle/ductile-behavior of the individual compounds. Liu *et al.* recently showed by studying differnt structure types for

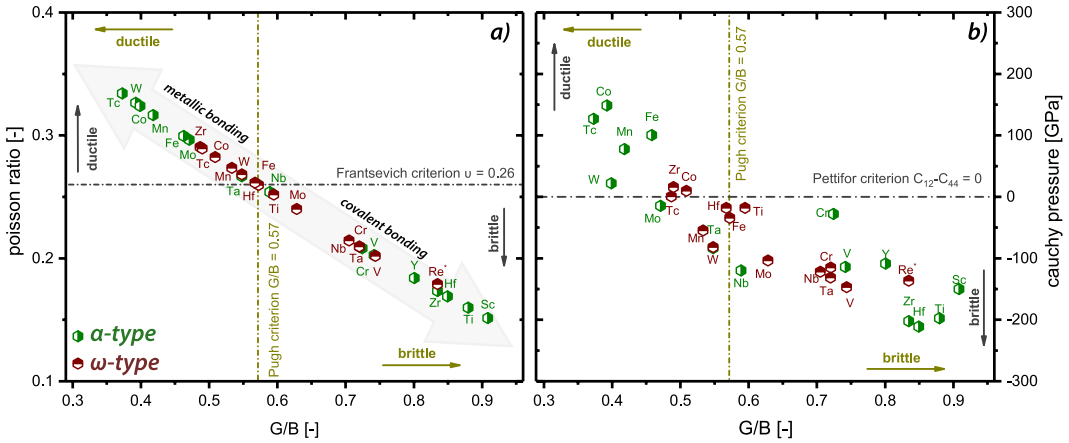

Figure 5. Pugh criterion (G/B-ratio) as a dependence of the Poisson ratio (Frantsevich criterion, (**a**)) and the Cauchy pressure (C_{12}–C_{44}), Pettifor criterion, (**b**). The green and red hexagons correspond to α- and ω-structure, respectively. (*ReB_2 in **a,b**) was taken from literature[50]. Please note, that some diborides have very similar values and are therefore overlapping.

WB_2, that α-structured WB_2 reveals smaller number of bonds accompanied by increased bond lengths. Therefore, α-WB_2 is predicted to obtain a decreased hardness compared to its ω-structured polymorph. This is in good agreement to our results stating that α-WB_2 shows a rather metallic bonding character than in its ω-structure, hence being in the highly ductile regime after all criteria.

Influence of vacancies on the phase stability of TMB_2. Because PVD promotes the formation of many point defects such as vacancies–and these mutually influence not just the preferred structure[28], mechanical properties[40], thermal properties[5], or magnetic properties[41], for example–the impact of TM as well as B vacancies on the phase stabilities of α-TMB_2 and ω-TMB_2 is studied. To optimize the supercell size, which should be large enough (to allow the calculation of low vacancy concentrations and to minimize their mutual interaction), supercells with $3 \times 3 \times 3$ (81 lattice sites) and $3 \times 3 \times 1$ (with 108 lattice sites) were used for α-TMB_2 and ω-TMB_2, respectively. Vacancies in these structures were created by removing either one boron or one TM atom, hence ~3.7 at.% TM and ~1.9 at.% B vacancies in α-TMB_2, and ~2.8 at.% TM and ~1.5 at.% B vacancies in ω-TMB_2.

For the ω-TMB_2 structure, the effect of B vacancies is studied for the flat and the puckered B plane individually. The energies of formation for such defected structures (E_f^{vac}), also calculated using Equation 1, are used to obtain the difference in E_f ($\Delta E_f = E_f^{vac} - E_f^{perf}$), presented in Fig. 6. Thus, if ΔE_f is positive, the formation of vacancies is energetically not preferred. Many of the α-TMB_2 compounds actually prefer the formation of vacancies, such as CrB_2, MnB_2, FeB_2, CoB_2 (3d), and MoB_2, TcB_2 (4d), and TaB_2, WB_2 (5d). Whereas CrB_2 and NbB_2 only prefer the formation of B vacancies, the other mentioned α-TMB_2 compounds prefer the formation of B as well as TM vacancies. Comparing Fig. 6a with Fig. 2 clearly shows that those α-TMB_2 compounds, which are metastable with respect to ω-TMB_2 (e.g. MnB_2, MoB_2, WB_2), favour the formation of vacancies, whereas those α-TMB_2 compounds, which are stable with respect to ω-TMB_2 do not want to have vacancies (e.g. TiB_2, ZrB_2, HfB_2). Although ΔE_f is also negative for NiB_2 (3d), and RuB_2, RhB_2, PdB_2 (4d), and OsB_2, IrB_2, PtB_2, AuB_2 (5d), these compounds still exhibit positive E_f^{vac} values, and are thus still chemically instable.

The majority of the TMB_2 compounds are chemically destabilized by vacancies in their ω-structure. Although ΔE_f is negative for CuB_2, CdB_2, OsB_2, and AuB_2, these compounds are still chemically unstable with E_f^{vac} being positive. ScB_2, TiB_2 (3d), and YB_2, ZrB_2 (4d), are interesting compounds, as the formation of B-vacancies is only preferred at the puckerd planes, whereas for MnB_2, FeB_2 (3d), TcB_2, RuB_2, (4d), and WB_2 (5d), the formation of B-vacancies is only preferred at the flat planes.

If we consider those TMB_2 compounds that exhibit a metastale α-TMB_2 (with respect to ω-TMB_2) without defects, the preference for ω-TMB_2 or α can alter when introducing vacancies. In this respect, we only concentrate on those TMB_2 compounds that are chemically stable (i.e., negative E_f values), even when introducing defects (i.e., still negative E_f^{vac} values), which are CrB_2, MnB_2, FeB_2, CoB_2 (3d), and MoB_2, TcB_2(4d), and TaB_2, WB_2 (5d). As for these compounds ΔE_f is always more negative for the α- than for the ω-structure, the two structures come closer in E_f with introducing vacancies. For TaB_2, already the 3.7 at.% TM and 1.9 at.% B vacancies considered in this study, the α-structure overrules the ω-structure. For 2.8 at.% TM vacancies or 1.4 at.% B vacancies, ω-WB_2 is still slightly preferred over the α-WB_2 relative, but the difference significantly decreases from ~25 meV/at (no vacancies) to ~21 meV/at. Thus, we propose that the defects induced by PVD processes are responsible for the preferred formation of α-WB_2[33,34] rather than the chemically more stable ω-WB_2, if no defects are considered.

Designing ternary $TM(I)_{1-x}TM(II)_xB_2$ thin film materials. Several experimental studies on WB_2 report the formation of the α-structure when deposited as thin film via physical vapor deposition[16,42,43]. Taking into account the results presented before, where α-WB_2 is located in the ductile regime (for all criteria), this compound is the ideal candidate for designing ternary borides. Furthermore, finding a good alloying element

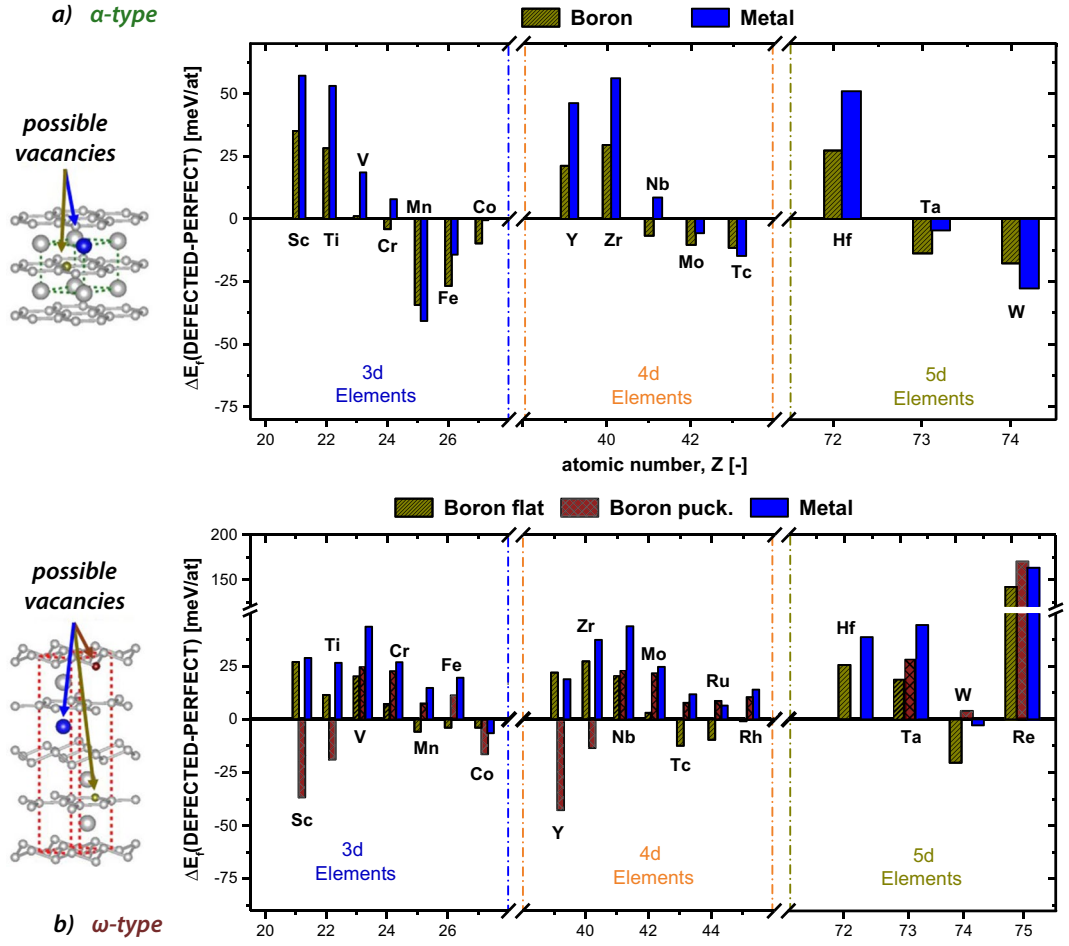

Figure 6. (**a**) Energies of formation per vacancy for all TMB_2 crystallizing in α structured cells. The yellow hatched bars indicate the energies of formation of a randomly taken boron vacancy. The blue bars represent the values for a randomly taken metal vacancy. (**b**) Energies of formation per vacancy for all TMB_2 crystallizing in ω. The yellow and red hatched bars indicate the energies of formation of a randomly taken boron vacancy on the flat and puckered planes. The blue bars represent the values for a randomly taken metal vacancy.

â€“ with respect to matching lattice constants (equilibrium volume), high bulk modulus, similar tendency for vacancies, and lower E_f - TaB_2 points out as an excellent candidate for stabilizing the structure with low cost on ductility. Figure 7, shows the vacancy impact on the α- and ω-structure in the ternary $W_{1-x}Ta_xB_{2-z}$ system (see Fig. 7a) and the impact of shottky (stoichiometric) defects on the binary systems (see Fig. 7b,c). Clearly, the data for the α-structure reveals the favor in stabilizing the structure via vacancies decreasing with increasing Ta content. Contrary to low Ta contents, where the structure strongly desires metal defects, the structure even gets slightly destabilized at high Ta contents for metal vacancies. The small discrepancy to the data presented in Fig. 6 is based on the uncertainty (in the range of 1 to 2 meV/at) of the calculations and the use of different SQS supercells. However, B vacancies stabilize in the full compositional range the α structure (also negative E_f for all compositions investigated). Especially for α-TaB_2, this is in good agreement to experimental studies showing a slight boron deficiency[44]. For α-WB_2, no experimental studies regarding the chemical composition have been conducted so far.

For the ω-structure the trends for increasing Ta contents remain, whereas the different vacancy types destabilize the structure. Exceptions here are boron vacancies (flat layer) at high W contents where a (insignificant) gain in energy can be obtained. Considering the results for shottky defects (see Fig. 7b,c) introduced in the α- and ω-structure for the binaries, it can be clearly seen, that the α-structure is more stable at $\geq$7.5 at.% vacancies and in the range of $0 > x \geq 22.5$ at.% for WB_2 and TaB_2, respectively. In respect to the concept shown in Fig. 1, the data suggests to start experimental work on $W_{1-x}Ta_xB_2$ thin films. These films should be strongly stabilized due to alloying (low Ta content) and the implementation of vacancies. Furthermore, the material should show a rather ductile behavior compared to "classical" diborides like TiB_2. Preliminary experimental studies on single-phased DC magnetron sputtered α-$W_{1-x}Ta_xB_2$ (with x = 0, 0.07, 0.14, 0.26) thin films showed, that by annealing in vacuum the decomposition of the α-phase is postponed with increasing Ta content from 800–1000 °C (α-WB_2) to 1200–1400 °C (α-$W_{0.74}Ta_{0.26}B_2$). Additionally, micromechanical bending tests of cantilevers revealed a small decrease in fracture toughness for increasing Ta content from ~3.7 $MPa\sqrt{m}$ (α-WB_2) to ~3.0 $MPa\sqrt{m}$ (α-$W_{0.74}Ta_{0.26}B_2$).

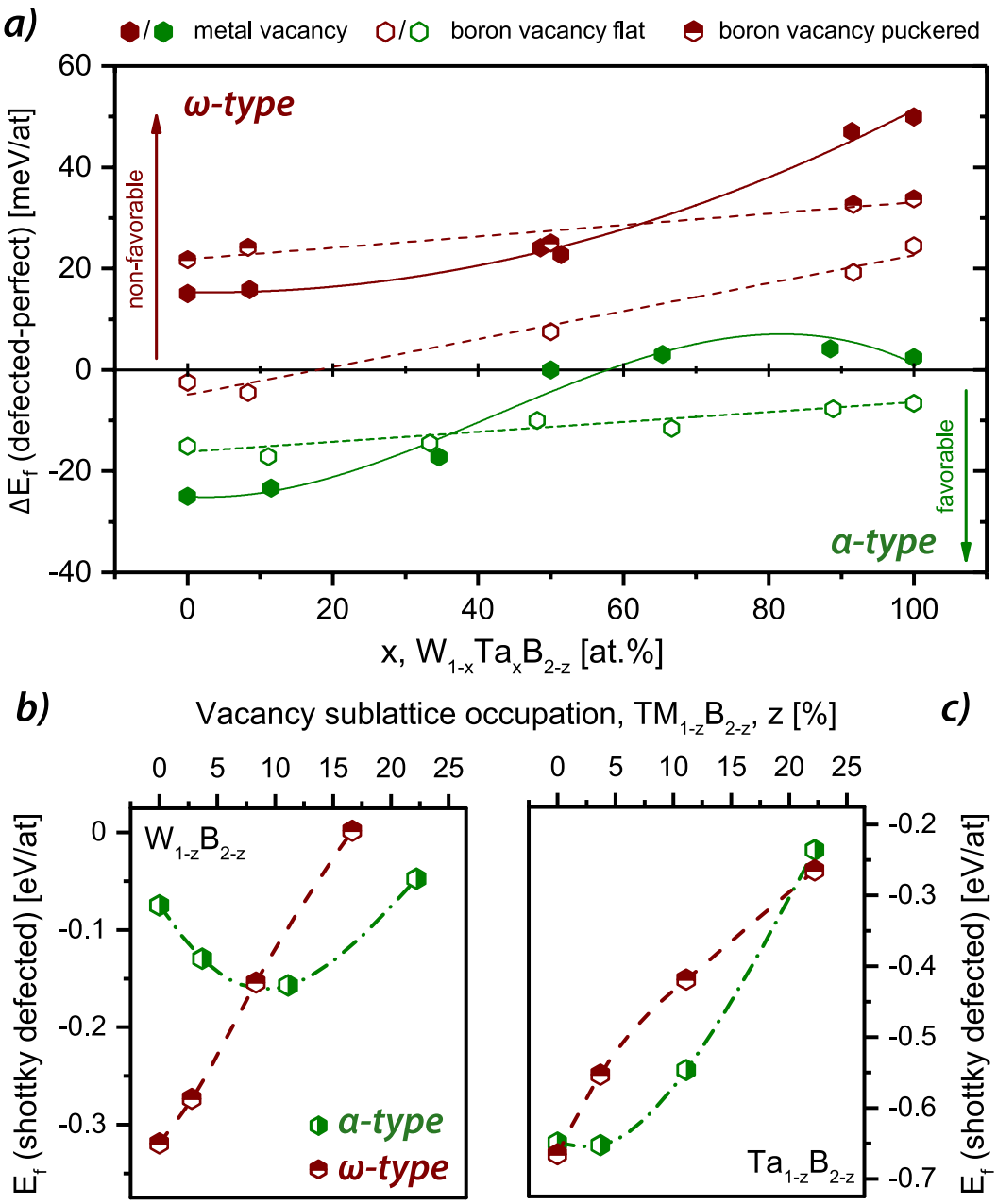

Figure 7. Impact of metal and boron (flat (open symbols) and puckered (half filled symbols) vacancies on the stability of α- and ω-structured $W_{1-x}Ta_xB_{2-z}$ depending on the Ta/(Ta + W) ratio (**a**). Impact of vacancy concentration (shottky defects) on E_f of the two discussed structures for WB_2 (**b**) and TaB_2 (**c**). The green and dark red symbols correspond to the α- and ω-structure, respectively.

Conclusion

Summarizing the results, we have confirmed the tendency of early TMB_2 compounds preferring the α-structure due to their lower E_f values compared to the ω-structure. TMB_2 compounds with higher atomic numbers in their period than VB_2 (3d), NbB_2 (4d), and HfB_2 (5d) reveal more chemical stability in the ω-structure.

The equilibrium volume of the individual elements in the α-structure is throughout smaller compared to their ω-structured counterpart due to the absence of the puckered boron planes. Moreover, it decreases with atomic radii up to that transition metal where E_f becomes positive. Regarding the bulk moduli, the opposite trend compared to the equilibrium volume is shown reaching its maxima for α-CrB_2 (3d), α-MoB_2 (4d), and α-ReB_2 (5d). Based on our studies on point defects, we can conclude, that diborides where the α-structure is chemically more stable than the ω-structure are destabilized when introducing metal or boron vacancies. Furthermore, ScB_2, TiB_2, YB_2, and ZrB_2 prefer the formation of vacancies on the puckered boron plane when considering the ω-structure which underlines their strong tendency to crystallize in the α-structure.

After applying three different criteria (Frantsevich, Pugh, and Pettifor) on the mechanical properties obtained from the calculation of the full elastic tensor, α-MnB_2, α-FeB_2, α-CoB_2, α-TcB_2, and α-WB_2 are classified as

ductile diborides. Hence, these are all TMB_2 in the α-structure, where the ω-structure shows more chemical stability due to the more negative E_f value.

Based on our calculations we propose α-$W_{1-x}Ta_xB_{2-z}$ as a promising ternary material system, providing excellent mechanical strength as well as ductility. WB_2 only provides excellent ductility data (according to the three ductility criteria) when stabilized in the metastable α-structure (AlB_2-type). With the addition of vacancies (which are typical for physical vapor deposited materials) the α-structure becomes energetically preferred over the ω-structure (W_2B_{5-x} type). TaB_2 exhibits almost the same energy of formation for the α-as well as ω-structure, and again significantly better ductility data for the α-structure. Only the Pettifor criterion indicates α-TaB_2 as brittle whereas the other two criteria (Pugh and Frantsevich) indicate α-TaB_2 as ductile. Thus, the addition of Ta is predicted to further promote the stabilization of α-WB_2 structure with relatively low costs in ductility.

Methods

Applying density functional theory (DFT) coded in VASP (Vienna Ab Initio Simulation Package)[45,46] using the projector augmented waves method within the generalized gradient approximation (PAW-PBE)[47], structure and stability of transition metal diborides (TMB_2) were studied. To avoid human errors, the calculations were semi-automated prepared and analyzed for all TM-Borides using python- and bash-scripting, respectively. 28 transition metals were considered, including all 3d, 4d and 5d elements except for Mercury (In case of Re the calculation of elastic constants for the α- and ω-structure exceeded the chosen time limit for computational effort as the compound was studied in detail in literature[18,19]). Therefore, all energy cutoffs and k-point meshes, where carefully chosen to ensure energy convergence of a few meV/at. The lattice parameter, the equilibrium volume and bulk moduli where fitted using a Birch-Murnaghan fit. To calculate the single-crystal elastic constants the method suggested by R. Yu *et al.*[48] was obtained. Furthermore, the formation energy of single vacancies where studied using the Alloy-Theoretic Automated Toolkit[49] where in the case of α-structure $3 \times 3 \times 3$ supercells containing 81 Atoms and $3 \times 3 \times 1$ supercells containing 108 atoms for the ω-structure where created. For the α-structure one - either metal or boron site - was eliminated which corresponds to a vacancy concentration of ~3.7 at.% and ~1.9 at.%, respectively. However, concerning the ω-structure, the two different boron sites (flat and puckered) as well as the metal site where taken into account interrelated to ~1.4 at.% boron vacancies and ~2.8 at.% metal vacancies.

Data availability. The datasets generated and analysed during the current study are available from the corresponding author on reasonable request.

References

1. Rodgers, J. R. & Cebon, D. Materials informatics. *MRS Bull.* **31**, 975–980 (2006).
2. Ivanovskii, A. L. Mechanical and electronic properties of diborides of transition 3d–5d metals from first principles: Toward search of novel ultra-incompressible and superhard materials. *Prog. Mater Sci.* **57**, 184–228 (2012).
3. Mayrhofer, P. H., Tischler, G. & Mitterer, C. Microstructure and mechanical/thermal properties of Cr-N coatings deposited by reactive unbalanced magnetron sputtering. *Surf. Coat. Technol.* **142–144**, 78–84 (2001).
4. Mitterer, C., Mayrhofer, P. H. & Musil, J. Thermal stability of PVD hard coatings. *Vacuum* **71**, 279–284 (2003).
5. Moraes, V. *et al*. Thermal conductivity and mechanical properties of AlN-based thin films. *J. Appl. Phys.* **119** (2016).
6. Mayrhofer, P. H. *et al*. Self-organized nanostructures in the Ti-Al-N system. *Appl. Phys. Lett.* **83**, 2049–2051 (2003).
7. Willmann, H. *et al*. Thermal stability of Al-Cr-N hard coatings. *Scr. Mater.* **54**, 1847–1851 (2006).
8. Chen, L., Holec, D., Du, Y. & Mayrhofer, P. H. Influence of zr on structure, mechanical and thermal properties of Ti-Al-N. *Thin Solid Films* **519**, 5503–5510 (2011).
9. Mayrhofer, P. H., Hovsepian, P. E., Mitterer, C. & Münz, W.-D. Calorimetric evidence for frictional self-adaptation of TiAlN/VN superlattice coatings. *Surf. Coat. Technol.* **177–178**, 341–347 (2004).
10. Hahn, R. *et al*. Superlattice effect for enhanced fracture toughness of hard coatings. *Scr. Mater.* **124**, 67–70 (2016).
11. Mitterer, C. Borides in thin film technology. *J. Solid State Chem.* **133**, 279–291 (1997).
12. Kayhan, M. *et al.* Neutron diffraction and observation of superconductivity for tungsten borides, WB and W_2B_4. *Solid State Sci.* **14**, 1656–1659 (2012).
13. Mayrhofer, P. H., Mitterer, C., Wen, J. G., Greene, J. E. & Petrov, I. Self-organized nanocolumnar structure in superhard TiB_2 thin films. *Appl. Phys. Lett.* **86**, 1–3 (2005).
14. Nedfors, N. *et al*. Superhard NbB_{2-x} thin films deposited by dc magnetron sputtering. *Surf. Coat. Technol.* **257**, 295–300 (2014).
15. Euchner, H. & Mayrhofer, P. H. Designing thin film materials - ternary borides from first principles. *Thin Solid Films* **583**, 46–49 (2015).
16. Euchner, H. *et al*. Solid solution hardening of vacancy stabilized $Ti_xW_{1-x}B_2$. *Acta Mater.* **101**, 55–61 (2015).
17. Alling, B., Högberg, H., Armiento, R., Rosen, J. & Hultman, L. A theoretical investigation of mixing thermodynamics, age-hardening potential, and electronic structure of ternary $M^1_{1-x}M^2_xB_2$ alloys with AlB_2 type structure. *Sci. Rep.* **5**, 9888 (2015).
18. Chung, H.-Y. *et al*. Synthesis of ultra-incompressible superhard rhenium diboride at ambient pressure. *Science* **316**, 436–439 (2007).
19. Feng, S. *et al*. Ab initio study on structural, electronic properties, and hardness of re-doped W_2B_5. *Solid State Commun.* **245**, 60–64 (2016).
20. Feng, S. *et al*. Theoretical investigations of physical stability, electronic properties and hardness of transition-metal tungsten borides WB_x(x = 2.5, 3). *Chem. Phys. Lett.* **635**, 205–209 (2015).
21. Rachbauer, R. *et al*. Decomposition pathways in age hardening of Ti-Al-N films. *J. Appl. Phys.* **110** (2011).
22. Euchner, H. & Mayrhofer, P. H. Vacancy-dependent stability of cubic and wurtzite $Ti_{1-x}Al_xN$. *Surf. Coat. Technol.* **275**, 214–218 (2015).
23. Klimashin, F. F., Koutná, N., Euchner, H., Holec, D. & Mayrhofer, P. H. The impact of nitrogen content and vacancies on structure and mechanical properties of Mo–N thin films. *J. Appl. Phys.* **120**, 185301 (2016).
24. Perry, A. J. On the existence of point defects in physical vapor deposited films of TiN, ZrN, and HfN. *J. Vac. Sci. Technol. A* **6**, 2140–2148 (1988).
25. Christel, P., Meunier, A., Heller, M., Torre, J. P. & Peille, C. N. Mechanical properties and short-term *in-vivo* evaluation of yttrium-oxide-partially-stabilized zirconia. *J. Biomed. Mater. Res.* **23**, 45–61 (1989).
26. Gregoire, J. M., Kirby, S. D., Turk, M. E. & van Dover, R. B. Structural, electronic and optical properties of (Sc,Y)N solid solutions. *Thin Solid Films* **517**, 1607–1609 (2009).
27. Ma, L. *et al.* Phase stability, anisotropic elastic properties and electronic structures of C15-type Laves phases ZrM_2 (M = Cr, Mo and W) from first-principles calculationss. *Philos. Mag.* **97**, 2406–2424 (2017).

28. Dahlqvist, M., Jansson, U. & Rosen, J. Influence of boron vacancies on phase stability, bonding and structure of MB_2 (M = Ti, Zr, Hf, V, Nb, Ta, Cr, Mo, W) with AlB_2 type structure. *J. Phys. Condens. Matter* **27** (2015).
29. Vajeeston, P., Ravindran, P., Ravi, C. & Asokamani, R. Electronic structure, bonding, and ground-state properties of AlB_2-type transition-metal diborides. *Phys. Rev. B Condens. Matter* **63**, 045115 (2001).
30. Liu, D., Duan, Y. & Bao, W. Correlation between electronic structure, mechanical properties and phase stability in intermetallic compounds. *Ceram. Int.* (2018).
31. Ravindran, P. & Asokamani, R. Correlation between electronic structure, mechanical properties and phase stability in intermetallic compounds. *Bull. Matter. Sci.* **20**, 10185 (1997).
32. Wang, X.-B., Tian, D.-C. & Wang, L.-L. The electronic structure and chemical stability of the AlB_2-type transition-metal diborides. *J. Phys. Condens. Matter* **6** (1999).
33. Fahrenholtz, W. G., Hilmas, G. E., Talmy, I. G. & Zaykoski, J. A. Refractory Diborides of Zirconium and Hafnium. *J. Am. Ceram. Soc.* **90**, 1347–1364 (2007).
34. Frotscher, M. *et al.* M2B5 or M2B4? A Reinvestigation of the Mo/B and W/B System. *Anorg. Allg. Chem.* **633**, 2626–2630 (2007).
35. Otani, S., Ohashi, H. & Ishizawa, Y. Solid solution ranges of zirconium diboride with other refractory diborides: HfB_2, TiB_2, TaB_2, NbB_2, VB_2 and CrB_2. *J. Alloys. Compd.* **221**, L8–L10 (1995).
36. Pettifor, D. G. Theoretical predictions of structure and related properties of intermetallics. *Mater. Sci. Technol.* **8**, 345–349 (1992).
37. Ali, M. A., Hadi, M. A., Hossain, M. M., Naqib, S. H. & Islam, A. K. M. A. Theoretical investigation of structural, elastic, and electronic properties of ternary boride MoAlB. *Phys. Status Solidi* (2017).
38. Mir, S. H. *et al.* Static and dynamical properties of heavy actinide monopnictides of lutetium. *Sci. Rep.* **6**, 29309 (2016).
39. Pugh, S. F. XCII. relations between the elastic moduli and the plastic properties of polycrystalline pure metals. *The London, Edinburgh, Dublin Philos. Mag. J. Sci.* **45**, 823–843 (1954).
40. Sammalkorpi, M., Krasheninnikov, A., Kuronen, A., Nordlund, K. & Kaski, K. Mechanical properties of carbon nanotubes with vacancies and related defects. *Phys. Rev. B Condens. Matter* **70**, 245416 (2004).
41. Venkatesan, M., Fitzgerald, C. B. & Coey, J. M. D. Thin films: unexpected magnetism in a dielectric oxide. *Nat.* **430**, 630 (2004).
42. Woods, H. P., Wawner, F. E. Jr. & Fox, B. G. Tungsten diboride: preparation and structure. *Science* **151**, 75 (1966).
43. Jiang, C. *et al.* Preparation and characterization of superhard AlB_2-type WB_2 nanocomposite coatings. *Phys. Status Solidi* **210**, 1221–1227 (2013).
44. Motojima, S. & Sugiyama, K. Chemical vapour deposition of tantalum diboride. *J. Mater. Sci.* **14**, 2859–2864 (1979).
45. Kresse, G. & Joubert, D. From ultrasoft pseudopotentials to the projector augmented-wave method. *Phys. Rev. B Condens. Matter* **59**, 1758–1775 (1999).
46. Kresse, G. & Furthmüller, J. Efficient iterative schemes for ab initio total-energy calculations using a plane-wave basis set. *Phys. Rev. B Condens. Matter* **54**, 11169–11186 (1996).
47. Perdew, J. P., Burke, K. & Ernzerhof, M. Generalized gradient approximation made simple. *Phys. Rev. Lett.* **77**, 3865–3868 (1996).
48. Yu, R., Zhu, J. & Ye, H. Q. Calculations of single-crystal elastic constants made simple. *Comput. Phys. Commun.* **181**, 671–675 (2010).
49. van de Walle, A., Asta, M. & Ceder, G. The alloy theoretic automated toolkit: A user guide. *CALPHAD* **26**, 539–553 (2002).
50. Hao, X. *et al.* Low-compressibility and hard materials ReB_2 and WB_2: Prediction from first-principles study. *Phys. Rev. B Condens. Matter* **74**, 224112 (2006).

Acknowledgements

The computational results presented have been achieved using the Vienna Scientific Cluster (VSC). The financial support by the Austrian Federal Ministry of Economy, Family and Youth and the National Foundation for Research, Technology and Development is gratefully acknowledged. We also thank for the financial support of Plansee Composite Materials GmbH and Oerlikon Balzers, Oerlikon Surface Solutions AG. The authors state that the project is funded within the framework of the Christian Doppler Laboratory for Application Oriented Coating Developement which is partly supported by the Austrian Federal Ministry of Economy, Family and Youth and the National Foundation for Research, Technology and Development. The conducted research was carried out within this framework including the cooperation between the Laboratory (located at TU Wien) and Oerlikon Surface Solutions AG as well as Plansee Composite Materials GmbH. The authors acknowledge the TU Wien University Library for financial support through its Open Access Funding Program.

Author Contributions

V.M., D.H. and P.H.M. conceived the present idea. V.M. and F.C. performed the calculations. V.M., H.R. and P.H.M. analyzed the data and shaped the study, especially creating all figures and text. All authors (V.M., H.R., C.F., P.P., H.B., D.H. and P.H.M.) discussed the results, provided critical feedback and contributed to the manuscript.

Additional Information

Supplementary information accompanies this paper at https://doi.org/10.1038/s41598-018-27426-w.

Competing Interests: V.M., R.H., C.F., D.H. and P.H.M. are funded by the Christian Doppler Laboratory. P.P. and H.B. are employees of the cooperating companies Plansee Composite Materials GmbH and Oerlikon Surface Solutions AG, respectively.

Publisher's note: Springer Nature remains neutral with regard to jurisdictional claims in published maps and institutional affiliations.